

1 **Effects of grain size and seawater salinity on magnesium hydroxide**
2 **dissolution and secondary calcium carbonate precipitation kinetics:**
3 **implications for ocean alkalinity enhancement**

4 Charly A. Moras^{1*}, Tyler Cyronak², Lennart T. Bach³, Renaud Joannes-Boyau¹ and Kai G. Schulz¹
5
6

7 ¹Faculty of Science and Engineering, Southern Cross University, Lismore, NSW, Australia

8 ²Institute for Coastal Plain Science, Georgia Southern University, Savannah, GA, USA

9 ³Ecology & Biodiversity, Institute for Marine and Antarctic Studies, University of Tasmania, Hobart, TAS, Australia
10

11 *Correspondence:* Charly A. Moras (c.moras.10@student.scu.edu.au)
12

13 **Abstract.** Understanding the impact that mineral grain size and seawater salinity have on magnesium hydroxide ($\text{Mg}(\text{OH})_2$)
14 dissolution and secondary calcium carbonate (CaCO_3) precipitation is critical for the success of ocean alkalinity enhancement.
15 We tested the $\text{Mg}(\text{OH})_2$ dissolution kinetics in seawater using three $\text{Mg}(\text{OH})_2$ grain sizes (<63, 63-180 and >180 μm) and at
16 three salinities (~36, ~28 and ~20). While $\text{Mg}(\text{OH})_2$ dissolution occurred quicker the smaller the grain size, salinity did not
17 significantly impact measured rates. Our results also demonstrate that grain size can impact secondary CaCO_3 precipitation,
18 suggesting that an optimum grain size exists for ocean alkalinity enhancement (OAE) using solid $\text{Mg}(\text{OH})_2$. Of the three grain
19 sizes tested, the medium grain size (63-180 μm) was optimal in terms of delaying secondary CaCO_3 precipitation. We
20 hypothesize that in the lowest grain size experiments, the higher surface area provided numerous CaCO_3 precipitation nuclei,
21 while the slower dissolution of bigger grain size maintained a higher alkalinity ~~and~~ pH at the surface of particles, increasing
22 CaCO_3 precipitation rates and making it observable much quicker than for the intermediate grain size. Salinity also played a
23 role in CaCO_3 precipitation where the decrease in magnesium (Mg) allowed for secondary precipitation to occur more quickly,
24 similar in effect size to another known inhibitor, i.e., dissolved organic carbon (DOC). In summary, our results suggest that
25 OAE efficiency as influenced by CaCO_3 precipitation not only depends on seawater composition but also on the physical
26 properties of the alkaline feedstock used.

27

1. Introduction

The concentration of carbon dioxide (CO₂) in the atmosphere has been in a relatively narrow band from ~180 to ~280 ppmv for the last 800,000 years, but has risen rapidly over the last 250 years to approximately 420 ppmv today (Lüthi et al., 2008, Monnin et al., 2001, Siegenthaler et al., 2005). This is the result of increasing utilisation of fossil fuels, cement production and land-use change, driving subsequent global climate change (IPCC, 2021). While about 42% of CO₂ emissions remain in the atmosphere, and are mainly responsible for global warming, about 26% are currently absorbed by the oceans, leading to ocean acidification (Friedlingstein et al., 2022, IPCC, 2021). To locally mitigate the effects of ocean acidification and slow down the increase in Earth's global temperature, CO₂ reduction efforts are not sufficient and the use of carbon dioxide removal (CDR) strategies have become necessary as a supplement to emission reduction (Hoegh-Guldberg et al., 2019).

One emerging marine CDR approach is ocean alkalinity enhancement (OAE). Over long timescales, the natural CO₂-facilitated weathering of alkaline rocks supplies alkalinity to the oceans, influencing its CO₂ uptake potential and storage. OAE builds upon this weathering feedback in the Earth System and can be accomplished by actively spreading pulverized alkaline minerals in and around marine environments or electrochemically removing acidity from seawater (Eisaman et al., 2023). In both cases, the seawater total alkalinity (TA) is increased thereby increasing the storage capacity of seawater for atmospheric CO₂ (GESAMP, 2019, Khesghi, 1995). On local scales around where the OAE perturbation is made, the increase in alkalinity and pH may also mitigate ocean acidification (Hartmann et al., 2013).

Recent studies have investigated the carbonate chemistry changes following OAE, and a major outcome was the risk for runaway calcium carbonate (CaCO₃) precipitation (Fuhr et al., 2022, Hartmann et al., 2023, Moras et al., 2022). There are several inorganic CaCO₃ precipitation mechanisms that have been described in the literature (Morse et al., 2007, Pytkowicz, 1965). CaCO₃ can precipitate homogeneously in the absence of solid or soluble organic and inorganic particles, pseudo-homogeneously in the presence of organic surfaces, and heterogeneously in the presence of mineral solids (Marion et al., 2009). The key parameter that governs whether precipitation occurs is the calcium carbonate saturation state (Ω), which is calculated from seawater Ca²⁺ and CO₃²⁻ concentrations as:

$$\Omega = \frac{[Ca^{2+}][CO_3^{2-}]}{K_{sp}}$$

where [Ca²⁺] and [CO₃²⁻] are the concentrations of calcium and carbonate in solution, respectively, and K_{sp} the solubility product of CaCO₃ in the solution. Ω is therefore closely related to the composition of the solution and its salinity, but is also highly temperature dependent (Zeebe and Wolf-Gladrow, 2001). For aragonite, the CaCO₃ morphotype that inorganically

57 precipitates in modern seawater, the saturation state (Ω_A) has to be higher than 12.3 for pseudo-homogeneous precipitation to
58 occur in water with a salinity of 35 and at 25 °C (Marion et al., 2009). Homogeneous precipitation will occur at much higher
59 Ω_A values, while heterogeneous precipitation will occur already at much lower Ω_A but depends on the actual lattice
60 compatibility of CaCO_3 for the mineral particles present (Morse et al., 2007, Zhong and Mucci, 1989). Another important
61 aspect is that once precipitation becomes measurable, it will continue in a “runaway” fashion, i.e., quickly ramping up until it
62 slows down once Ω_A gets closer to 1 again.

63 Several studies have reported such behaviour upon mineral alkalinity addition (Fuhr et al., 2022, Hartmann et al.,
64 2023, Moras et al., 2022) with critical threshold of Ω_A of ~ 7.0 for the two calcium based OAE minerals of calcium oxide –
65 CaO – and calcium hydroxide – $\text{Ca}(\text{OH})_2$ – and report precipitation stopping at Ω_A values of 1.8-2.0 (Moras et al., 2022).
66 Precipitation has also been observed for magnesium-based minerals such as brucite or reagent grade magnesium hydroxide –
67 $\text{Mg}(\text{OH})_2$, but actual thresholds have not been determined (Hartmann et al., 2023). Furthermore, the effect of grain size,
68 determining factor of the surface area available for mineral dissolution and CaCO_3 precipitation, has not been studied.
69 Similarly, the effect of potential CaCO_3 precipitation inhibitors such as seawater magnesium (Mg) concentrations, governed
70 by salinity, and dissolved organic carbon (DOC), are relatively unknown (Chave and Suess, 1970, Millero et al., 2001, Pan et
71 al., 2021, Zhong and Mucci, 1989). This study focuses on the impact of $\text{Mg}(\text{OH})_2$ grain size on its dissolution kinetics in
72 natural seawater, as well as the impact of salinity. Furthermore, the subsequent runaway CaCO_3 precipitation that is triggered,
73 and its kinetics are reported. Finally, the effect of increased [Mg] and [DOC] in seawater on the CaCO_3 precipitation process
74 is explored.

75

76 2. Material and methods

77 2.1. Seawater collection and experimental setup

78 Seawater was collected in Broken Head, New South Wales, Australia (25°42'12" S, 153°37'03" E) using 25 L jerry
79 cans, about 200 m from the shore to avoid sampling sand and suspended particles. The collected seawater was stored in the
80 dark at 4 °C for three days to reduce microbial activity and allow particles to settle to the bottom, facilitating filtration. The
81 entire contents of the jerry cans were then sterile filtered using a peristaltic pump and a 0.2 μm Whatman Polycap 75 AS filter,
82 before being stored in cleaned and autoclaved 25 L polycarbonate bottles. Prior to conducting the experiments, each seawater
83 batch was equilibrated to laboratory air pCO_2 by bubbling them with H_2O -saturated air for at least a week (Moras et al., 2023).
84 This ensured comparable starting conditions for the various experiments, with a calculated starting pCO_2 of $420.6 \pm 28.6 \mu\text{atm}$
85 in all experiments. All experiments utilised reagent grade $\text{Mg}(\text{OH})_2$ (>98%, kindly supplied by Atlas Materials) which had
86 been ground in a Pulverizer laboratory mill.

87

88 2.2. Grain size and salinity experiments

89 Approximately 1.5 litres of seawater were placed in a clean 2 L borosilicate 3.3 beaker, surrounded by a water jacket
90 set to 21 °C and controlled by a tank chiller line TK-1000. A floating lid with three ports was placed on the water surface,
91 allowing for concurrent Mg(OH)₂ addition, pH measurement and water sampling. Upon Mg(OH)₂ addition, the seawater was
92 incubated for 18 hours to allow for full Mg(OH)₂ dissolution. Thereafter the beaker content was transferred to a clean 1 L
93 borosilicate 3.3 Schott bottle which was tightly closed without any headspace to minimise CO₂ ingassing. The bottle was
94 placed on a stirring platform at 200 rpm in the dark, at room temperature (24.8 ±1.3 °C). All grain size and salinity treatments
95 were run in triplicates for up to 34 days.

96 For the grain size experiments, three grain size ranges were produced using two stainless steel sieves with 63 µm and
97 180 µm mesh sizes. The medium range, i.e., 63-180 µm, was also used for the salinity experiments at ~36, ~28 and ~20. The
98 lower salinity seawater was produced by mixing natural seawater with MilliQ water. Exact salinities were determined on 200
99 mL of seawater sample equilibrated to room temperature in a gas tight polycarbonate container, by measuring conductivity
100 and temperature with a 914 pH/conductometer, and converted to salinity using the 1978 practical salinity scale (Lewis and
101 Perkin, 1981). For all experiments, Mg(OH)₂ additions were adjusted to yield an Ω_A of ~9 (Table 1) to allow for a significant
102 TA increase and secondary CaCO₃ precipitation, based on previously found thresholds for CaO and Ca(OH)₂, and with the
103 assumption that the CaCO₃ inhibition role of Mg²⁺ requires a higher Ω_A for CaCO₃ precipitation within days (Moras et al.,
104 2022). Varying amount of Mg(OH)₂ were used in the salinity experiments. The decrease in dissolved [Ca] following dilution
105 with MilliQ led to higher amounts of Mg(OH)₂ to be added with decreasing salinity to reach a similar Ω_A of about 9.
106 Furthermore, preliminary tests conducted with the Mg(OH)₂ powder used for these experiments, despite having reagent grade
107 properties (>98% pure), have shown that only about 75% of the theoretical maximum TA was generated. Therefore, the
108 Mg(OH)₂ additions were adjusted accordingly, with additions varying from 23.3 mg kg⁻¹ in the salinity 36 experiments (and
109 all grain size experiments) to 30.2 mg kg⁻¹ in the salinity 20 experiments.

Formatted: Subscript

110 In all the experiments, the first 18 hours of reaction were monitored by measuring the pH on the free scale (pH_F) with
111 an Aquatrode Plus with Pt1000 (Metrohm) connected to an 888 Titrande (Metrohm), before transferring the content of the 2
112 L beaker into the clean 1 L Schott bottles. A sample for TA and DIC measurements was taken before Mg(OH)₂ addition, and
113 after the 18 hours. The temperature and pH_F were then recorded twice a day until a sudden drop in pH_F was observed, linked
114 to CaCO₃ precipitation. A new sample for TA and DIC measurements was then taken. The time at which CaCO₃ runaway
115 precipitation was deemed to have started was considered to be the last stable pH_F measurement before the sudden drop. TA
116 and DIC samples were taken at varying intervals during CaCO₃ precipitation (see figures 2 and 4) to cover most of the CaCO₃
117 precipitation process, and at least 300 mL of water was reserved for two TA and DIC samples at the end of the experiment.

118 Between 9 and 10 TA and DIC samples per experiment were collected to monitor the changes in DIC and TA overtime. Their
119 decrease in a 2:1 ratio was further used to reconstruct TA and DIC from pH measurements in the experiments on the effect of
120 Mg and DOC on CaCO₃ precipitation (see below for details).

121
|

Table 1. Summary of the main experimental parameters for each of the incubations investigating the salinity and grain size effects on Mg(OH)₂ dissolution and CaCO₃ precipitation kinetics.

Experimental details	TA increase ($\mu\text{mol kg}^{-2}$)	Maximum O ₂ reached	Days of stable TA	Overall TA loss ($\mu\text{mol kg}^{-2}$)	Overall DIC loss ($\mu\text{mol kg}^{-2}$)	Final O ₂
Salinity effect on Mg(OH)₂ dissolution and CaCO₃ precipitation kinetics						
<i>Salinity-35-80</i>						
Rep 1; Rep 2; Rep 3	555.5; 500.4; 534.9	9.23; 8.96; 9.16	10; 12; 9	1409.8; 1013.9; 1068.5	414.8; 477.4; 467.7	2.04; 1.95; 1.84
Mean \pm St. Dev.	530.3 \pm 27.8	9.12 \pm 0.14	10.33 \pm 1.53	1030.8 \pm 32.8	456.7 \pm 27.9	1.94 \pm 0.10
<i>Salinity-28-47</i>						
Rep 1; Rep 2; Rep 3	618.7; 660.9; 615.8	9.18; 9.48; 9.29	6; 6; 4	1460.9; 1104.8; 1096.8	487.0; 494.5; 529.5	1.74; 1.68; 1.63
Mean \pm St. Dev.	631.8 \pm 25.3	9.32 \pm 0.16	5.33 \pm 1.15	1487.5 \pm 23.4	503.5 \pm 22.8	1.68 \pm 0.05
<i>Salinity-20-38</i>						
Rep 1; Rep 2; Rep 3	575.9; 591.2; 605.3	8.26; 8.49; 9.14	2; 2; 1	899.3; 963.3; 1062.9	481.4; 522.8; 603.6	1.54; 1.51; 1.50
Mean \pm St. Dev.	590.8 \pm 14.7	8.63 \pm 0.45	1.67 \pm 0.58	975.2 \pm 82.4	535.9 \pm 62.1	1.52 \pm 0.02
Grain size effect on Mg(OH)₂ dissolution and CaCO₃ precipitation kinetics						
<i>Small Grain size</i>						
Rep 1; Rep 2; Rep 3	422.9; 447.5; 412.1	8.60; 8.48; 8.22	7; 4; 3	1419.3; 1021.9; 988.3	562.2; 547.3; 550.6	2.06; 2.16; 2.14
Mean \pm St. Dev.	427.5 \pm 18.1	8.43 \pm 0.20	4.67 \pm 2.08	1409.8 \pm 18.7	553.4 \pm 7.8	2.12 \pm 0.05
<i>Medium Grain size</i>						
Rep 1; Rep 2; Rep 3	555.5; 500.4; 534.9	9.23; 8.96; 9.16	10; 12; 9	1409.8; 1013.9; 1068.5	414.8; 477.4; 467.7	2.04; 1.95; 1.84
Mean \pm St. Dev.	530.3 \pm 27.8	9.12 \pm 0.14	10.33 \pm 1.53	1030.8 \pm 32.8	456.7 \pm 27.9	1.94 \pm 0.10
<i>Large Grain size</i>						
Rep 1; Rep 2; Rep 3	368.9; 272.3; 412.6	8.41; 7.92; 8.72	3; 3; 2	1432.8; 980.7; 1103.1	606.1; 661.4; 647.5	1.89; 1.90; 2.02
Mean \pm St. Dev.	351.3 \pm 71.8	8.35 \pm 0.40	2.67 \pm 0.56	1438.9 \pm 61.4	638.3 \pm 28.8	1.93 \pm 0.07

Table 1: Summary of the main experimental parameters for each of the incubations investigating the salinity and grain size-effects on $Mg(OH)_2$ dissolution and $CaCO_3$ precipitation kinetics. "Days of stable TA" encompasses the time between maximum ΔTA recorded and the start of $CaCO_3$ runaway precipitation.

Experimental details	Starting Conditions			Conditions after Full Dissolution			End Conditions	
	Starting TA ($\mu\text{mol kg}^{-1}$)	Starting DIC ($\mu\text{mol kg}^{-1}$)	TA increase ($\mu\text{mol kg}^{-1}$)	Maximum Ω_A reached	Days of stable TA	Overall TA loss ($\mu\text{mol kg}^{-1}$)	Overall DIC loss ($\mu\text{mol kg}^{-1}$)	Final Ω_A
<i>Salinity effect on $Mg(OH)_2$ dissolution and $CaCO_3$ precipitation kinetics</i>								
Salinity 36 (35.80)	2292.2 \pm 1.4	2046.40 \pm 0.88	530.27 \pm 27.82	9.12 \pm 0.14	10.33 \pm 1.53	1030.76 \pm 32.79	456.71 \pm 27.91	1.97 \pm 0.02
Salinity 28 (28.47)	1845.4 \pm 1.5	1686.35 \pm 0.55	631.79 \pm 25.26	9.32 \pm 0.04	5.33 \pm 1.15	1087.48 \pm 23.38	505.92 \pm 21.66	1.68 \pm 0.05
Salinity 20 (20.38)	1323.2 \pm 3.1	1246.08 \pm 0.53	590.83 \pm 14.69	8.63 \pm 0.17	1.67 \pm 0.58	975.15 \pm 82.41	535.92 \pm 62.12	1.52 \pm 0.01
<i>Grain size effect on $Mg(OH)_2$ dissolution and $CaCO_3$ precipitation kinetics</i>								
Small (<63 μm)	2300.0 \pm 1.0	2048.18 \pm 0.50	427.48 \pm 18.11	8.43 \pm 0.02	4.67 \pm 2.08	1009.85 \pm 18.67	553.35 \pm 7.79	2.12 \pm 0.02
Medium (63-180 μm)	2292.2 \pm 1.4	2046.40 \pm 0.88	530.27 \pm 27.82	9.12 \pm 0.14	10.33 \pm 1.53	1030.76 \pm 32.79	456.71 \pm 27.91	1.97 \pm 0.02
Large (> 180 μm)	2317.3 \pm 0.6	2056.78 \pm 1.74	351.25 \pm 71.78	8.35 \pm 0.04	2.67 \pm 0.58	1038.88 \pm 61.40	638.31 \pm 28.76	1.93 \pm 0.02

Formatted: Font: (Default) Times New Roman, 14 pt, Bold

Formatted: Font: 14 pt

Formatted: Font: 14 pt

Formatted: Font: 14 pt

Formatted Table

Formatted: Font: 11 pt, Not Bold

Formatted: Font: 14 pt

Formatted: Font: 11 pt

Formatted: Font: 11 pt, Not Bold

Formatted: Font: 11 pt, Not Bold

Formatted: Font: 11 pt, Italic

Formatted: Font: 10 pt, Italic

Formatted: Font: 11 pt

Formatted: Font: 11 pt

Formatted: Font: 11 pt

Formatted: Font: 11 pt, Italic

Formatted: Font: 10 pt, Italic

Formatted Table

Formatted: Font: 11 pt

Formatted: Font: 11 pt

Formatted: Font: 11 pt

Formatted: Font: 11 pt

Formatted: Font: 11 pt

Formatted: Font: 11 pt

Formatted: Font: 11 pt

Formatted: Font: 11 pt

Formatted: Font: 11 pt

Formatted: Font: 11 pt

Formatted: Font: 11 pt

Formatted: Font: 11 pt

Formatted: Font: 11 pt

Formatted: Font: 11 pt

Formatted: Font: 11 pt

Formatted: Font: 11 pt

Formatted: Font: 11 pt

Formatted: Font: 11 pt

Formatted: Font: 11 pt

Formatted: Font: 11 pt

Formatted: Font: 11 pt

Formatted: Font: 11 pt

Formatted: Font: 11 pt

Formatted: Font: 11 pt

Formatted: Font: 11 pt

Formatted: Font: 11 pt

Formatted: Font: 11 pt

Formatted: Font: 12 pt, English (Australia)

Formatted: Indent: First line: 0 cm

2.3. Manipulation of dissolved inorganic carbon and magnesium

The seawater dilution by MilliQ to decrease salinity also decreased the concentration of various seawater components, such as Mg and DOC concentrations. To disentangle a potentially general effect of salinity on $\text{Mg}(\text{OH})_2$ dissolution and secondary precipitation kinetics from reductions in Mg and DOC concentrations, two additional experiments were designed. In the first, the experiments at a salinity of 20 were replicated, but the Mg concentration was increased to a concentration representative for a salinity of 35, i.e., $52.8 \text{ mmol kg}^{-1}$ (Dickson et al., 2007), by magnesium chloride (MgCl_2) addition from a 3 M stock solution (molarity verified by inductively coupled plasma mass spectrometer measurements). This experiment was run in triplicate. For the second experiment, a DOC-enriched seawater solution at the salinity of 20 was produced by ultrafiltration (molecular weight cut-off of 2,000 Daltons, Vivaflow200 Hydrosart, Sartorius). A DOC gradient was then created in five bottles by mixing the DOC-enriched salinity 20 seawater with the MilliQ-diluted seawater. The DOC concentrations ranged from approximately $120 \text{ } \mu\text{mol kg}^{-1}$ to approximately $325 \text{ } \mu\text{mol kg}^{-1}$.

In both the Mg and DOC experiments, dissolution and secondary CaCO_3 precipitation kinetics were mainly monitored by pH_f measurements, although a sample for TA and DIC was also taken before $\text{Mg}(\text{OH})_2$ addition and at the end of each treatment. These samples, coupled to the pH_f measurements, allowed the changes in TA and DIC to be estimated over time. The reconstruction occurred in two steps, where the increase in pH following $\text{Mg}(\text{OH})_2$ was assumed to be linked to an increase of TA at constant DIC. Then, any decrease in pH was assumed to be due to CaCO_3 precipitation, so the estimated TA and DIC loss after $\text{Mg}(\text{OH})_2$ dissolution were decreasing in a 2:1 ratio, as observed in the salinity and grain size experiments. Finally, to account for CO_2 ingassing over time, the difference between estimated maximum TA and final measured TA was used as a proxy. Half of the difference, representing CaCO_3 precipitation, was used to estimate the theoretical DIC loss. Once compared to the final measured DIC, an ingassing rate was estimated.

2.4. Analytical procedures

The pH electrode was calibrated using three Metrohm buffer solutions (pH 4, 7 and 9), corresponding to a pH measurement on the free scale. TA analyses were conducted using a potentiometric titration with an 848 Titrino Plus, coupled to an 869 Compact Sample Changer from Metrohm. A 0.05M HCl solution with the ionic strength adjusted to 0.72 mol kg^{-1} (representative for a salinity of 35) using NaCl was used as the titrant (Dickson et al., 2007). The DIC concentration was measured using an Automated Infra-Red Inorganic Carbon Analyzer (AIRICA) coupled to a LI-COR Li7000 Infra-Red detector (Gafar and Schulz, 2018). Both TA and DIC measurements were corrected against in-house reference material (previously calibrated against certified reference material), with measurement uncertainties of ± 2.20 and $\pm 1.98 \text{ } \mu\text{mol kg}^{-1}$ (Moras et al., 2023). Ω_A and carbonate chemistry speciation were calculated from measured TA and DIC, providing temperature and salinity measurements, using CO2SYS (Sharp et al., 2021). To do so, the boric acid dissociation constant

Formatted: Section start: New page

155 [from Uppström \(1974\), the carbonic acid dissociation constant from Lueker et al. \(2000\), and the sulfuric acid dissociation](#)
156 [constant of Dickson \(1990\) were selected.](#)

157 For scanning electron microscopy (SEM), discrete samples of about 10 mL of TA enriched seawater were filtered
158 through 0.2 µm polycarbonate filters (Whatman Cyclopore). These filters were rinsed with 20 mL of MilliQ to remove salts
159 and dried overnight at 60 °C. Once dried, the filters were kept in a desiccator until analysis. The filters were attached to double-
160 sided carbon tabs and placed on aluminium mounts before being coated with gold. SEM analysis was performed using a
161 tabletop Scanning Electron Microscope TM4000 Plus from Hitachi, coupled to an Energy Dispersive X-Ray (EDX) Analyser,
162 allowing to determine the elemental composition of observed particles.

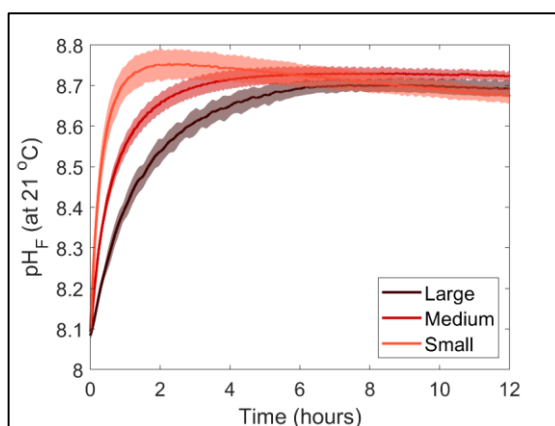
163 The concentration of the MgCl₂ stock solution was measured by inductively coupled plasma mass spectrometer (ICP-MS)
164 measurements using an Agilent 7700 ICP-MS, coupled to a laser ablation unit (NWR213, Electro Scientific Industries, Inc.).
165 Seawater reference materials from the National Research Council of Canada NASS-6 were used to correct the measurements.
166 The DOC concentration of the DOC-enriched stock solution was determined using a Thermo Fisher Flash Elemental Analyzer
167 after acidifying the sample with nitric acid (Carvalho, 2023).

Formatted: Indent: First line: 0.63 cm

169 3. Results

170 3.1. Grain size effects on Mg(OH)₂ dissolution kinetics

171 Three Mg(OH)₂ grain sizes were dissolved in seawater at a salinity of ~36 (Figure 1). The starting pH_F was similar
172 for all incubations, with 8.11 ±0.03, 8.09 ±0.01 and 8.07 ±0.03, for the small (<63 µm), medium (63-180 µm) and large (>180
173 µm) grain sizes, respectively. Upon dissolution, pH_F increased quite rapidly, reaching a maximum after about two hours for
174 the small particle size experiments, and about 6 to 8 hours in the medium and large particle size experiments (Figure 1). In
175 each incubation, a logarithmic trend in pH_F was observed, with the dissolution being much quicker for smaller grain sizes.
176 After two hours, the maximum pH_F recorded for the smaller grain size was 8.76 ±0.04, which continuously decreased to 8.68
177 ±0.00 between 11 and 12 hours after Mg(OH)₂ addition. In contrast, the pH_F for the medium and larger grain size increased to
178 8.72 ±0.00 and 8.68 ±0.03 after about eight hours and remained stable thereafter, respectively (Figure 1).



180
181 **Figure 1: Changes in pH_F at 21 °C following dissolution of three $Mg(OH)_2$ grain sizes in natural seawater over 12 hours. Each grain**
182 **size was run in triplicate, with the average presented as the solid lines and the standard deviation range as the transparent areas.**

183 184 3.2. Grain size effect on $CaCO_3$ precipitation kinetics

185 The pH increase was reflected by increasing TA, measured prior to the $Mg(OH)_2$ addition and 18 hours later, by about
186 430, 530 and 350 $\mu\text{mol kg}^{-1}$, in the small, medium and large grain size incubations, respectively (Figure 2). The TA remained
187 stable for 3-7 days, 9-12 days, and 2-3 days before dropping in each grain size treatment (small, medium, large). In all
188 incubations, TA concentrations decreased in a similar fashion, with a strong drop the first two days, before slowly decreasing
189 for another week and stabilising. The overall TA loss for the duration of the experiments was $\sim 1035 \mu\text{mol kg}^{-1}$ in the medium
190 and large grain size incubations, while the TA dropped by about $1010 \mu\text{mol kg}^{-1}$ in the small grain size incubations (Table 1).

191 The changes in Ω_A followed a similar pattern as TA, increasing from ~ 2.8 on average to ~ 9.1 in the medium grain
192 size incubation, and to ~ 8.4 in the small and large grain size experiments. Ω_A dropped at the same time as TA in the respective
193 experiments, stabilising around ~ 2.0 in all experiments.

194 Finally, a small drop in DIC was observed after $Mg(OH)_2$ addition in all experiments, of about 80, 30 and 140 μmol
195 kg^{-1} in the small, medium and large grain size incubations, respectively. The DIC remained then relatively stable until the rapid
196 TA drop, where the overall DIC drops for the small, medium and large grain size incubations were calculated at ~ 550 , ~ 455
197 and $\sim 640 \mu\text{mol kg}^{-1}$, respectively. While TA and Ω_A remained stable after this drop, DIC slightly increased, particularly
198 obvious in the medium and larger grain size incubations.

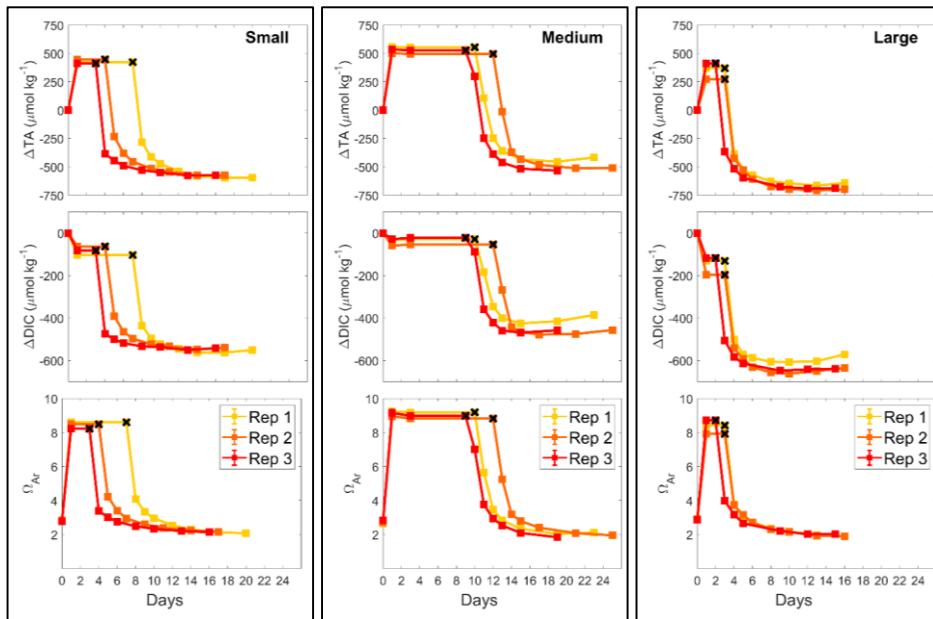


Figure 2: Changes in TA, DIC and Ω_A during dissolution of three $Mg(OH)_2$ grain sizes in natural seawater over up to 25 days. Three replicates were conducted for each grain size and are represented in red, orange and yellow. The last stable TA and DIC conditions estimated by pH_F measurements are represented by a black cross.

3.3. Salinity effect on $Mg(OH)_2$ dissolution kinetics

To test the salinity effect on $Mg(OH)_2$ dissolution and $CaCO_3$ precipitation kinetics, three sets of experiments were conducted in three different salinities, i.e., 20.38, 28.47 and 35.80, and using medium grain size $Mg(OH)_2$. From here on the salinities 20.38, 28.47 and 35.80 will be referred to as salinities 20, 28 and 36, respectively. Similarly to the grain size experiments, the dissolution of $Mg(OH)_2$ occurred rapidly in all three salinities, with the maximum pH_F being recorded after approximately 8 hours (Figure 3). Starting pH_F were slightly different, recorded at 7.99 ± 0.05 , 8.06 ± 0.01 and 8.09 ± 0.01 in the salinity 20, 28 and 36 incubations, and increased to a maximum of $9.19, \pm 0.00$, 8.91 ± 0.00 and 8.72 ± 0.00 , respectively. In all incubations, similar logarithmic trends were observed for pH_F (Figure 3).

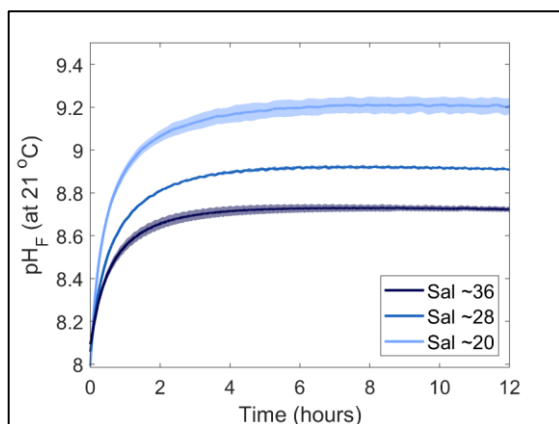


Figure 3: Changes in pH_F at 21 °C following $\text{Mg}(\text{OH})_2$ dissolution in three different seawater salinities over 12 hours. Each salinity has been run in triplicate, with the average presented as the solid lines and the standard deviation range as the transparent areas. Please note that different maximum pH levels were reached because of increasing $\text{Mg}(\text{OH})_2$ additions with decreasing salinity to reach a similar Ω_A .

3.4. Salinity effect on CaCO_3 precipitation kinetics

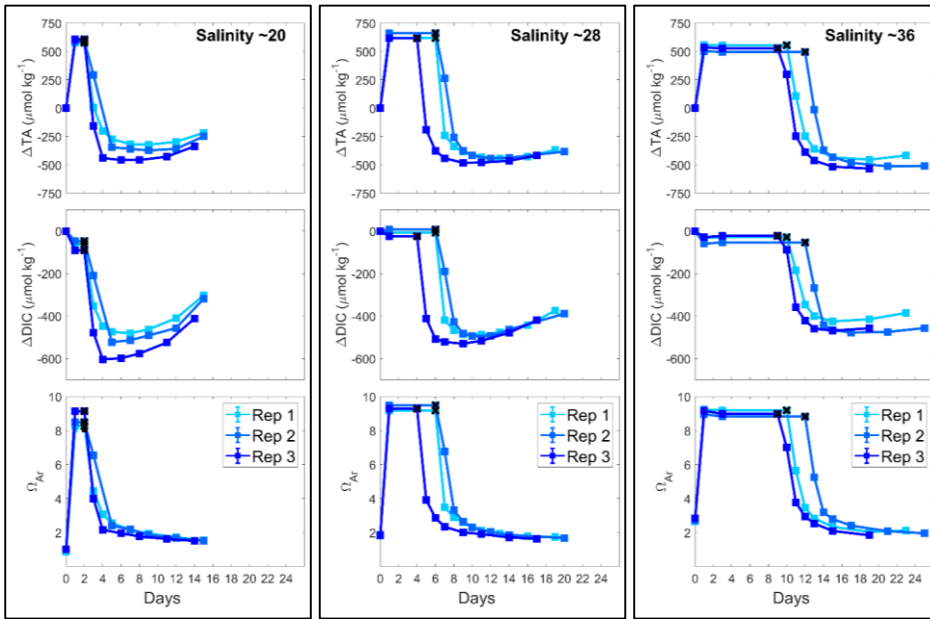
In all incubations, TA was increased as suggested by the pH_F trends, by ~ 590 , ~ 630 and $\sim 530 \mu\text{mol kg}^{-1}$ in the salinity 20, 28 and 36 incubations, respectively (Figure 4). The TA remained stable for different periods of time in each treatment; 1-2 days in the salinity 20 incubations, 4-6 days in the salinity 28 incubations, and 9-12 days in the salinity 36 incubations. Thereafter, TA dropped quickly the first two days in all incubations and stabilised quickly in the salinity 20 experiments. In the salinity 28 incubations, the TA slowly decreased over five days after the first strong drop and stabilised, while in the salinity 36 experiments, the TA decreased slowly after the initial drop over seven days before stabilising. The overall TA losses for salinities 20, 28 and 36 experiments were estimated at ~ 975 , ~ 1090 and $\sim 1030 \mu\text{mol kg}^{-1}$, respectively (Table 1).

Ω_A values followed a similar pattern as TA in all experiments. The starting Ω_A were different, varying between 1.0 for the salinity 20 incubations to 2.0 and 2.8 for the salinity 28 and 36 incubations, respectively. Similarly, following $\text{Mg}(\text{OH})_2$ additions, Ω_A quickly increased to reach 8.6, 9.3 and 9.1 with increasing salinity. Together with TA, Ω_A eventually started dropping, and then stabilised at different values, around 1.5 for a salinity of 20, around 1.7 for a salinity of 28 and around 2.0 for a salinity of 36.

Finally, DIC also decreased upon $\text{Mg}(\text{OH})_2$ additions. An initial DIC drop was observed directly after $\text{Mg}(\text{OH})_2$ additions of about $60 \mu\text{mol kg}^{-1}$ at the lowest salinity and $30 \mu\text{mol kg}^{-1}$ at the highest salinity. At a salinity of 28, a much smaller DIC drop was observed in one replicate. After a period of stable DIC conditions, DIC also dropped in a similar fashion

236 as TA, with an overall DIC loss of about 535, 505 and 455 $\mu\text{mol kg}^{-1}$ from the lower to higher salinity incubations. While no
 237 DIC increase was observed towards the end of the experiment in the salinity 36 incubations, strong DIC increases were
 238 observed in the salinity 28 incubations and even more prominent ones in the salinity 20 incubations.

239



240

241 **Figure 4: Changes in TA, DIC and Ω_A during $\text{Mg}(\text{OH})_2$ dissolution in three different salinities over up to 25 days. Three replicates**
 242 **were conducted for each salinity and are represented in shades of blue. The last stable TA and DIC conditions estimated by pH_f**
 243 **measurements are represented by a black cross.**

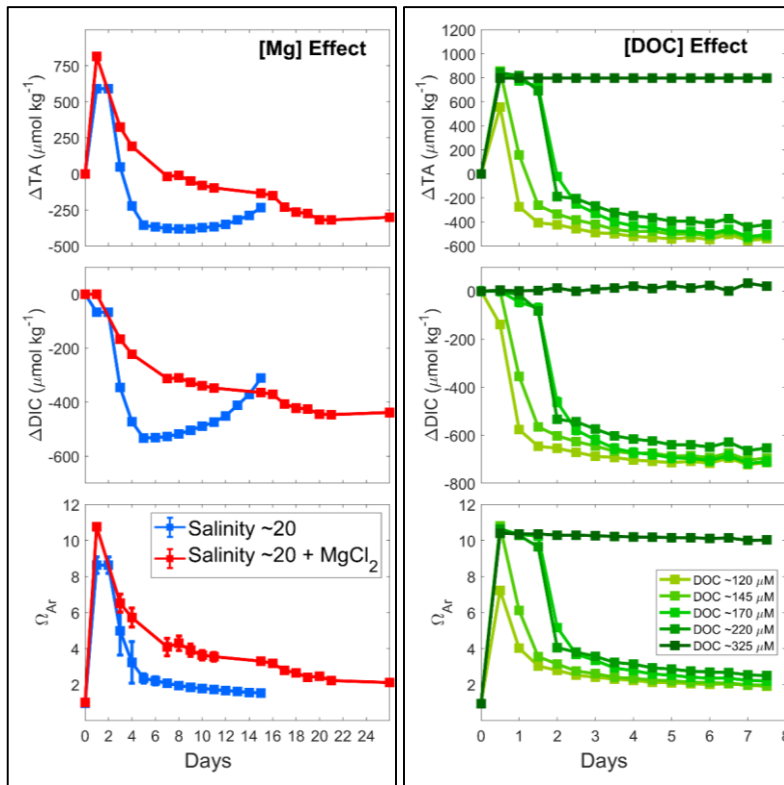
244

245 3.5. Magnesium and DOC effect on CaCO_3 precipitation

246 A similar pattern was observed for the salinity 20 experiments at natural and increased Mg concentrations, i.e., a rapid
 247 increase in TA reaching a maximum on day one, followed by a steady decline over the next two weeks (Figure 5). The
 248 maximum ΔTA reached was slightly different, with about 600 $\mu\text{mol kg}^{-1}$ of TA increase in the salinity 20, and nearly 800
 249 $\mu\text{mol kg}^{-1}$ in the salinity 20 + MgCl_2 incubations. Another interesting difference is the slower TA decrease with MgCl_2
 250 compared to the salinity 20. After about 18 days, the lowest ΔTA was reached while it only took about 6 days for the salinity
 251 20 ΔTA to reach the minimum. Similarly, DIC appeared to decrease less rapidly when MgCl_2 was present and Ω_A followed a
 252 similar trend after the initial strong increase.

253 Out of the five DOC experiments, four incubations showed a drop in TA (Figure 5). Similar maximum Δ TA were
 254 reached in most experiments, with a Δ TA of $\sim 800 \mu\text{mol kg}^{-1}$. However, in the incubation with $\sim 120 \mu\text{mol kg}^{-1}$ DOC, the TA
 255 increased only by $\sim 600 \mu\text{mol kg}^{-1}$. Following this increase, TA decreased within a day in both 120 and 145 $\mu\text{mol kg}^{-1}$ DOC
 256 incubations, and stayed stable until day 3 in incubations with 170 and 220 $\mu\text{mol kg}^{-1}$. These four incubations also show a
 257 similar levelling pattern over time, even though it appears that in the higher DOC incubations, the total loss in TA was lower
 258 than for the lower DOC incubations. Δ DIC also follow a similar trend to Δ TA, with an early drop at 120 $\mu\text{mol kg}^{-1}$ of DOC, a
 259 drop after one day at 145 $\mu\text{mol kg}^{-1}$ of DOC, and a slow decrease from day 1 and a stronger drop on day 2 at 170 and 220
 260 $\mu\text{mol kg}^{-1}$ of DOC. Ω_A followed a very similar pattern to Δ TA, with final Ω_A being higher in the experiments with higher DOC
 261 concentrations. Finally, in the experiment with the highest DOC concentration, i.e., 325 $\mu\text{mol kg}^{-1}$, no drop in TA, DIC or Ω_A
 262 was observed (the experiment was run for 42 days).

263



264

265 Figure 5: Comparison of the reconstructed-calculated TA, DIC and Ω_A changes at 21 °C following $\text{Mg}(\text{OH})_2$ addition in seawater
 266 with salinity of 20 (blue), and in seawater with salinity 20 and Mg concentration equal to a salinity 35 (red), and in seawater with

267 varying DOC concentrations (green). Values reported in the [Mg] Effect graphs represent the average of triplicate experiments run
268 at salinity 20 and salinity 20 + MgCl₂, with standard deviations represented by the error bars.

Formatted: Subscript

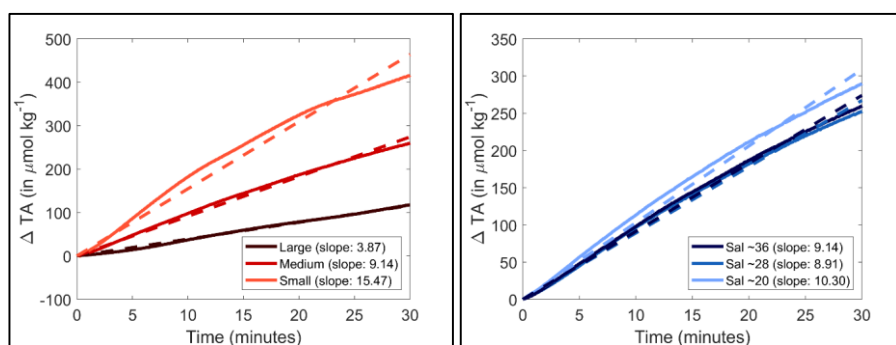
270 4. Discussion

271 4.1. Grain size and salinity effects on Mg(OH)₂ dissolution

272 Maximum Mg(OH)₂ dissolution directly after its addition was negatively correlated with grain size (Figure 1, Figure
273 3). The smaller the grain size, the faster the maximum pH_F is reached, indicative of complete dissolution. This can be explained
274 by the fact that smaller particles have a larger surface area per gram of material than larger ones. The increasing dissolution
275 rate with decreasing particle size is particularly noticeable in when TA changes were estimated by using the pH_F data and
276 starting DIC measurements (Figure 6). Assuming a constant DIC over the first 30 minutes of reaction, i.e., no significant
277 CaCO₃ precipitation and/or CO₂ ingassing, TA can be reconstructed using CO2SYS. The maximum ΔTA reached with the
278 larger particle size occurred within 8 hours while it only took about 2 hours for the ΔTA to reach a maximum with small
279 particle size. The initial dissolution rate, i.e., within the first 30 minutes, was also significantly different between the various
280 grain sizes. The TA generation of smaller grain size particles was estimated at about 796.5 ± 7.1 μmol of TA mg⁻¹ min⁻¹. The
281 medium particles dissolved about twice as slow over the first 30 minutes, estimated at 391.6 ± 2.6 μmol of TA mg⁻¹ min⁻¹,
282 while the larger grain sizes dissolved more than four times slower, with about 168.7 ± 6.9 μmol of TA mg⁻¹ min⁻¹. Another
283 important difference between the smaller grain size experiments and the two others is the constant decrease in pH_F observed
284 right after reaching the maximum pH_F value (Figure 1). This decrease in pH_F can only be linked to either CaCO₃ precipitation,
285 decreasing TA and ultimately pH_F, or CO₂ ingassing, increasing the dissolved CO₂ concentration and ultimately decreasing
286 the pH_F. The constant and linear trend suggest that the latter is responsible for the decrease. If CaCO₃ precipitation was
287 responsible for these pH_F changes, the changes would follow a similar pattern to a negative exponential function. This is due
288 to the fact that the more CaCO₃ nucleate, the more surface becomes available for further nucleation (Zhong and Mucci, 1989).
289 However, in our case, the changes appear linear. Such a pattern is indicative of CO₂ ingassing at an early stage, i.e., before the
290 ingassing starts plateauing, dictated by the difference between atmospheric and seawater pCO₂. Such ingassing is also
291 occurring in the other experiments, but is likely hidden by the stronger-pH_F increase occurring during the longer Mg(OH)₂
292 dissolution with bigger grain size.

293 For salinity, ~~we did not observe major differences in there was a difference in~~ initial dissolution rates within the range
294 of salinities tested, with dissolution rates for salinities 36, 28 and 20 estimated at 391.6 ± 2.6, 359.8 ± 0.2 and 301.9 ± 0.3 μmol
295 of TA mg⁻¹ min⁻¹, respectively. ~~While these differences are not as significant as those in the grain size experiments, the~~
296 ~~dissolution rate decreased by about 23% between salinity 36 and 20.~~ Overall, TA generation potential of smaller grain size
297 Mg(OH)₂ (<63 μm) at a salinity 36 was similar to that of Ca(OH)₂ (Moras et al., 2022) which was also sieved through 63 μm.
298 Assuming the same molar TA generation potential, the same maximum Ω_A should have been reached. However, for Ca(OH)₂

299 it was ~ 7.4 , while our small grain size $\text{Mg}(\text{OH})_2$ incubations reached a maximum Ω_A of ~ 8.4 . Such a difference is likely due
 300 to the difference in the starting conditions [and experimental settings](#). In the experiments shown here, the starting Ω_A was ~ 2.8
 301 while it was about ~ 2.5 in Moras et al. (2022). This is explained by the difference in the starting water composition and salinity,
 302 ultimately affecting the final Ω_A despite similar TA increases. [Furthermore, higher amounts of \$\text{Mg}\(\text{OH}\)_2\$ were added compared](#)
 303 [to Moras et al. \(2022\), leading to a higher \$\Omega_A\$ and a higher theoretical \$\Delta\text{TA}\$, if no early \$\text{CaCO}_3\$ nucleation occurred.](#) However,
 304 dissolution kinetics appear to differ between the minerals, with $\text{Ca}(\text{OH})_2$ dissolving within 20-30 minutes while it took two
 305 hours for $\text{Mg}(\text{OH})_2$. These two minerals still dissolve at a relatively quick pace compared to other OAE feedstocks, for instance
 306 olivine (Montserrat et al. 2017). Olivine took much longer to dissolve, with a maximum increase in pH recorded of ~ 0.15 units
 307 within 4-9 days. $\text{Ca}(\text{OH})_2$ and $\text{Mg}(\text{OH})_2$ additions required ~ 20 mg of materials, while to obtain such olivine results, more than
 308 30 g of olivine were added per kg of filtered seawater, meaning that the TA generation potential is several orders of magnitude
 309 lower.



312 **Figure 6:** Normalised changes in [calculated](#) TA over the first 30 minutes following $\text{Mg}(\text{OH})_2$ additions of three different grain sizes
 313 in natural seawater (left) and in three different salinities (right). A linear fit was calculated and is represented by the dashed line,
 314 and each slope is reported in the legend in between parentheses.

316 4.2. Grain size and salinity effect on CaCO_3 precipitation

317 In all experiments, $\text{Mg}(\text{OH})_2$ additions had been chosen to reach an Ω_A at which secondary CaCO_3 precipitation would
 318 be expected based on our experience with CaO and $\text{Ca}(\text{OH})_2$ (Moras et al., 2022). Based on our suspicion that CaCO_3 might
 319 precipitate on magnesium-rich particles less easily than onto calcium-rich particles we chose a saturation state of ~ 9 , slightly
 320 higher than the level of ~ 7 observed for CaO and $\text{Ca}(\text{OH})_2$ (Moras et al., 2022). Precipitation kinetics were similar for all grain
 321 sizes, i.e., after the first precipitation was observed a new steady state was achieved in about two weeks. Precipitation
 322 seemingly stopped at Ω_A values close to 2.0 in experiments with seawater at a salinity of 36, similar to observations made by

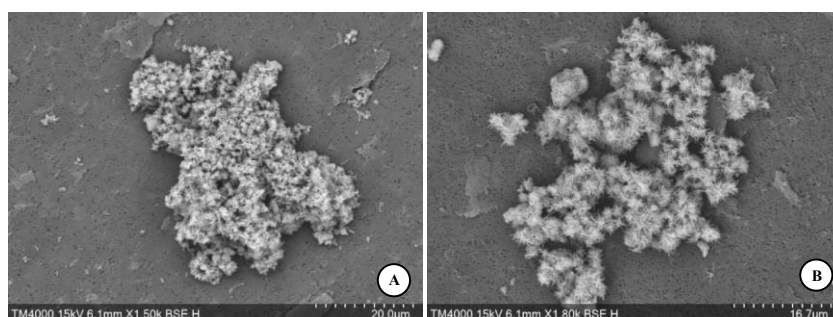
323 Moras et al. (2022) using CaO and Ca(OH)₂. For the smallest grain size, TA was stable for 3-7 days, which is longer than what
324 has been observed for CaO and Ca(OH)₂ at the same size (Moras et al., 2022). This could be related to higher lattice
325 compatibility of CaCO₃ for calcium-based minerals when it comes to precipitation onto mineral surfaces (Lioliou et al., 2007).
326 Interestingly, however, the rate at which CaCO₃ precipitated was similar for CaO and Mg(OH)₂, while Ca(OH)₂ took almost
327 twice as long to reach a new steady state (compare Figure 1 with Figure 2 in Moras et al., 2022).

328 TA remained stable for longer, i.e., 9-12 days with medium grain size. However, similarly to the smaller grain size
329 experiments, the TA was also less stable with the larger grain size, i.e., 2-3 days. As such, there appears to be an optimum
330 grain size for keeping TA stable for longer. To explain this, there must be two opposing processes at work. As discussed
331 earlier, smaller particles have larger surface area per gram of material than larger ones, i.e., smaller particles in our experiments
332 had on average more than 23 times the area of larger particles for the same amount of material, assuming round particles of 63
333 and 180 μm, respectively. Hence, heterogeneous precipitation will be quicker for smaller particles (Zhong and Mucci, 1989).
334 In contrast, what could favour quicker precipitation for larger particles with smaller surface area remains to be understood.
335 Here, it could be higher pH levels and hence Ω_A that are reached at a particle's surface as of having a larger diffusive boundary
336 layer. Hence, pH and Ω_A levels are likely to be much higher and remain for longer due to the slower dissolution of larger
337 particles at the site of CaCO₃ nucleation, which positively affects CaCO₃ precipitation rates.

338 At varying salinities, CaCO₃ precipitation became noticeable at different points in time, earlier at low salinity and
339 later at higher salinity. While the first assumption was that at lower salinity, the decrease in [Ca] would prevent early CaCO₃
340 precipitation in lower salinity, it appears that another mechanism is at play. The natural CaCO₃ inhibition potential of seawater,
341 due to dissolved Mg and DOC concentration, was affected during MilliQ dilution. It now appears that at lower salinity, the
342 decrease in inhibition allowed for CaCO₃ precipitation to occur despite a decrease in [Ca] and starting Ω_A . Under such
343 circumstances, early CaCO₃ nucleation on yet to be dissolved Mg(OH)₂ particles would occur at a faster rate in lower salinity
344 which could be explained by the early drops in DIC after Mg(OH)₂ addition. The absence of such decrease in the salinity 28
345 experiments is an interesting outcome but could be explained by an early CO₂ ingassing. The increase in DIC through CO₂
346 ingassing could have compensated for the DIC decrease from early CaCO₃ formation.

347 ~~To our surprise,~~ While EDX analysis did not reveal significant magnesium concentrations in early precipitated
348 aragonite crystals ~~to our surprise,~~ i.e., ~18 hours after Mg(OH)₂ addition, ~~some aragonite crystals were observed early on.~~ The
349 presence of Mg could have been expected if CaCO₃ precipitated heterogeneously onto Mg(OH)₂ particles (Figure 7). The
350 absence of Mg after EDX analysis suggests that while some Mg(OH)₂ could have been used as a precipitation nuclei for CaCO₃
351 early on, it completely dissolved within the first 18 hours. Only the freshly precipitation CaCO₃ would then remain in
352 suspension, eventually acting as precipitation nuclei for runaway CaCO₃ precipitation. Finally, it is interesting to highlight that
353 some traces of early aragonite crystals were present in all experiments, and that the needle-shaped crystals were two to three

354 times smaller in the larger grain size experiments than those sampled at the end of the medium grain size experiments (Figure
355 7). One explanation that supports the previously mentioned boundary layer theory is that the larger grain size particles,
356 dissolving at a slower pace, maintained a Mg-rich environment while CaCO_3 started nucleating. The presence of this Mg
357 during nucleation could have ultimately prevented CaCO_3 to fully form as bigger needle-like crystals. However, these are
358 speculations that are hard to prove or disprove.



360
361 **Figure 7: SEM images of aragonite crystals, sampled ~18 hours after larger $\text{Mg}(\text{OH})_2$ grain size addition (A) and sampled at the end**
362 **of the medium grain size incubations (B).**

364 4.3. The role of dilution and potential effects of Mg and DOC concentrations

365 The role of Mg in inhibiting CaCO_3 nucleation is well known (Morse et al., 2007, Pan et al., 2021, Pytkowicz, 1965).
366 Another known CaCO_3 nucleation inhibitor is organic matter, particularly dissolved organic matter (Chave and Suess, 1970).
367 While the role of organic matter is not as well understood as Mg, both have been linked to a decrease in CaCO_3 nucleation and
368 precipitation rates.

369 In our experiments involving dilution with MilliQ water, all dissolved components of the seawater were diluted,
370 including Mg and DOC. Such decreases could explain the quicker CaCO_3 precipitation in the salinity 20 experiments compared
371 to salinity 36, as lower Mg and DOC concentrations were not inhibiting precipitation as in the higher salinity treatments. To
372 test this, a new salinity 20 batch was prepared in triplicate and Mg was added to raise the total Mg concentration to $\sim 52 \text{ mmol}$
373 kg^{-1} , similar to the Mg concentration in natural seawater at a salinity 35. The Mg increase did affect CaCO_3 precipitation
374 kinetics as shown by changes in TA (Figure 5), being slightly slower and apparently reaching a new steady state at higher ΔTA
375 and Ω_A . Furthermore, it is important to highlight that despite CaCO_3 precipitation being triggered at a similar time, i.e., within
376 1 to 2 days, a difference was observed regarding the maximum ΔTA reached. In the salinity 20 + MgCl_2 experiments, the
377 maximum ΔTA value was higher than the one in the salinity 20 experiments. This suggests that with a higher dissolved Mg

378 concentration, less CaCO₃ is precipitated early on. Following this early precipitation, an overall slower precipitation rate is
379 observed until reaching a steady state (Figure 5).

380 However, the slightly reduced CaCO₃ precipitation rate due to decreased Mg concentrations alone cannot explain
381 such stark differences in TA stability between the salinity 36 and 20 experiments (Figure 4). It is most likely linked to both
382 the decrease in Mg and DOC concentrations when diluting with MilliQ. The gradient of five salinity 20 replicates with
383 increasing DOC concentrations clearly showed that secondary CaCO₃ precipitation could be delayed by modifying the DOC
384 concentrations alone. For instance, secondary precipitation became already measurable after 12 hours at DOC concentrations
385 of 120 μmol kg⁻¹, i.e., salinity 35 diluted to 20, but almost no secondary precipitation at a DOC concentration of 325 μmol kg⁻¹,
386 i.e., about one and a half times higher than in the salinity 35. CaCO₃ precipitation was delayed by about two days when
387 doubling DOC concentration, and completely prevented at even higher levels (Figure 5) within the timeframe of the experiment
388 (1 week). Together, these data suggest that seawater DOC and Mg act in synergy when it comes to inhibiting CaCO₃
389 precipitation.

390 Another interesting finding was the new steady state reached after runaway CaCO₃ precipitation. In natural seawater
391 at a salinity of 36, the equilibrated Ω_A was estimated around 2.0, which is about 0.8 units lower than the starting conditions
392 (Figure 4). The decrease in Ω_A after runaway precipitation has important implications for OAE, as when CaCO₃ precipitates
393 in a runaway fashion, seawater can become more acidic than it was prior to mineral dissolution and less able to sequester
394 atmospheric CO₂ (Moras et al., 2022). While further work is required to understand these carbonate chemistry mechanisms at
395 lower salinities, we can note that after runaway precipitation in seawater at a salinity of 20, the final Ω_A was higher than the
396 starting one. Such a difference is likely due to the lower starting Ca²⁺ concentration at lower salinity.

398 5. Conclusions

399 One main objective of this research was to assess the dissolution of Mg(OH)₂ in seawater at varying salinity, and
400 using different mineral grain sizes, and report on the subsequent CaCO₃ precipitation kinetics. The dissolution of Mg(OH)₂ in
401 natural seawater occurred at a much faster rate when using grain sizes lower than 63 μm, due to the higher surface area in
402 contact with seawater. In contrast, bigger particles (>63 μm) took about four times as long to fully dissolve. In all experiments,
403 CaCO₃ precipitation occurred in a runaway fashion, i.e. after a period of seeming stability, TA decreased rapidly before a new
404 steady state was reached at which TA reached concentrations far lower than prior to the Mg(OH)₂ addition. Such pattern was
405 also observed for Ca-rich minerals as well, but at lower Ω_A. While further research is required to precisely determine the
406 critical Ω_A for both Ca- and Mg-rich minerals, the longer time for CaCO₃ runaway precipitation to be initiated and the overall
407 higher Ω_A may suggest that Mg(OH)₂ is a safer alkaline feedstock for OAE. A-One major finding of this research was that two
408 processes seem to occur during CaCO₃ precipitation in relation to grain size, one where the higher surface area of smaller

409 particles ~~could~~ increase precipitation rates, while the second ~~may~~ maintains a higher pH around larger particles due to a larger
410 diffusive boundary layer compared to smaller particles, which increase~~s~~ precipitation rates. Hence, there appears to be an
411 optimum grain size to minimise secondary CaCO₃ precipitation. The second objective of this research was to understand the
412 role of salinity on Mg(OH)₂ dissolution and CaCO₃ precipitation kinetics. While no obvious changes in dissolution were
413 observed, CaCO₃ precipitation differed, with a quicker precipitation observed at lower salinities. The decrease in Mg
414 concentrations was identified as the root cause, although in our experiments it was also linked to a lowered DOC concentration,
415 an artefact of low salinity seawater preparation by dilution with MilliQ. Nevertheless, this highlights the importance of DOC
416 in modifying CaCO₃ precipitation kinetics and hence, TA stability.

418 Data availability

419 All data were collected by Charly A. Moras and were publicly published on the 05th of June 2024, on the open
420 repository ZENODO under the name "Dataset on the effects of mineral grain size and seawater salinity on Mg(OH)₂ dissolution
421 and CaCO₃ precipitation kinetics", and can be found at <https://doi.org/10.5281/zenodo.11483882>. All data will be made
422 available upon acceptance of the manuscript by *Biogeosciences*.

Formatted: Superscript

424 Author contributions

425 CAM and KGS designed the initial experiments with inputs from TC and LTB. CAM ran all the experiments and
426 with the help of KGS designed the follow-up experiments with MgCl₂ and DOC. The ICP-MS analyses were performed by
427 CAM and RJB, while CAM and KGS performed the SEM analyses. The first draft of the manuscript was written by CAM
428 with inputs from KGS, and all co-authors have helped writing and reviewing the manuscript for submission.

430 Competing interests

431 At least one of the (co-)authors is a member of the editorial board of *Biogeosciences*.

433 Acknowledgments

434 We would like to sincerely thank Atlas Materials for providing the magnesium hydroxide. We are also thankful to
435 Nick Ward for accommodating the use of the Scanning Electron Microscope, as well as Matheus Carvalho de Carvalho for the
436 dissolved organic carbon analyses.

438 **Financial support**

439 This research is part of the PhD project of Charly A. Moras that is funded by a Cat. 5 – SCU Grad School scholarship
440 from the Southern Cross University, Lismore, Australia. The ICP-MS analyses were made possible by Australian Research
441 Council grants to Renaud Joannes-Boyau and Kai G. Schulz (grant no. LE200100022) and to Renaud Joannes-Boyau (grant
442 no. LE120100201).

443

444 **References**

- 445 [Carvalho, M. C.: Adapting an elemental analyser to perform high-temperature catalytic oxidation for dissolved organic carbon](#)
446 [measurements in water, *Rapid Communications in Mass Spectrometry*, 37, e9451, 10.1002/rcm.9451, 2023.](#)
- 447 [Carvalho, M. C., Eickhoff, W., and Drexler, M.: Open-source autosampler for elemental and isotopic analyses of solids,](#)
448 [*HardwareX*, 8, e00123, 10.1016/j.ohx.2020.e00123, 2020.](#)
- 449 Chave, K. E. and Suess, E.: Calcium carbonate saturation in seawater: Effects of dissolved organic matter, *Limnology and*
450 *Oceanography*, 15, 633-637, 10.4319/lo.1970.15.4.0633, 1970.
- 451 [Dickson, A. G.: Standard potential of the reaction: \$\text{AgCl\(s\)} + 12\text{H}_2\text{\(g\)} = \text{Ag\(s\)} + \text{HCl\(aq\)}\$, and the standard acidity constant of](#)
452 [the ion \$\text{HSO}_4^-\$ in synthetic sea water from 273.15 to 318.15 K, *The Journal of Chemical Thermodynamics*, 22, 113-127,](#)
453 [10.1016/0021-9614\(90\)90074-Z, 1990.](#)
- 454 Dickson, A. G., Sabine, C. L., and Christian, J. R.: Guide to best practices for ocean CO₂ measurements, PICES Special
455 Publication 3; IOCCP Report 8, Sidney, British Columbia, North Pacific Marine Science Organization, 191 pp.,
456 10.25607/OBP-1342, 2007.
- 457 Eisaman, M. D., Geilert, S., Renforth, P., Bastianini, L., Campbell, J., Dale, A. W., Foteinis, S., Grasse, P., Hawrot, O.,
458 Löscher, C. R., Rau, G. H., and Rønning, J.: Assessing the technical aspects of ocean-alkalinity-enhancement approaches,
459 Guide to Best Practices in Ocean Alkalinity Enhancement Research, 2-oae2023, 3, 10.5194/sp-2-oae2023-3-2023, 2023.
- 460 Friedlingstein, P., Jones, M. W., O'Sullivan, M., Andrew, R. M., Bakker, D. C. E., Hauck, J., Le Quééré, C., Peters, G. P.,
461 Peters, W., Pongratz, J., Sitch, S., Canadell, J. G., Ciais, P., Jackson, R. B., Alin, S. R., Anthoni, P., Bates, N. R., Becker, M.,
462 Bellouin, N., Bopp, L., Chau, T. T. T., Chevallier, F., Chini, L. P., Cronin, M., Currie, K. I., Decharme, B., Djeutchouang, L.
463 M., Dou, X., Evans, W., Feely, R. A., Feng, L., Gasser, T., Gilfillan, D., Gkritzalis, T., Grassi, G., Gregor, L., Gruber, N.,
464 Gürses, Ö., Harris, I., Houghton, R. A., Hurtt, G. C., Iida, Y., Ilyina, T., Lujckx, I. T., Jain, A., Jones, S. D., Kato, E., Kennedy,
465 D., Klein Goldewijk, K., Knauer, J., Korsbakken, J. I., Körtzinger, A., Landschützer, P., Lauvset, S. K., Lefèvre, N., Lienert,
466 S., Liu, J., Marland, G., McGuire, P. C., Melton, J. R., Munro, D. R., Nabel, J. E. M. S., Nakaoka, S. I., Niwa, Y., Ono, T.,
467 Pierrot, D., Poulter, B., Rehder, G., Resplandy, L., Robertson, E., Rödenbeck, C., Rosan, T. M., Schwinger, J., Schwingshackl,
468 C., Séférian, R., Sutton, A. J., Sweeney, C., Tanhua, T., Tans, P. P., Tian, H., Tilbrook, B., Tubiello, F., van der Werf, G. R.,
469 Vuichard, N., Wada, C., Wanninkhof, R., Watson, A. J., Willis, D., Wiltshire, A. J., Yuan, W., Yue, C., Yue, X., Zaehle, S.,
470 and Zeng, J.: Global carbon budget 2021, *Earth System Science Data*, 14, 1917-2005, 10.5194/essd-14-1917-2022, 2022.
- 471 Fuhr, M., Geilert, S., Schmidt, M., Liebetrau, V., Vogt, C., Ledwig, B., and Wallmann, K.: Kinetics of Olivine Weathering in
472 Seawater: An Experimental Study, *Frontiers in Climate*, 4, 10.3389/fclim.2022.831587, 2022.
- 473 Gafar, N. A. and Schulz, K. G.: A three-dimensional niche comparison of *Emiliania huxleyi* and *Gephyrocapsa oceanica*:
474 reconciling observations with projections, *Biogeosciences*, 15, 3541-3560, 10.5194/bg-15-3541-2018, 2018.

475 GESAMP: High level review of a wide range of proposed marine geoengineering techniques. (Boyd, P.W. and Vivian, C.M.G.,
476 eds.). (IMO/FAO/UNESCO-IOC/UNIDO/WMO/IAEA/UN/UN Environment/UNDP/ISA Joint Group of Experts on the
477 Scientific Aspects of Marine Environmental Protection). Rep. Stud. GESAMP No. 98, 144 p.1020-4873, 2019.

478 Gore, S., Renforth, P., and Perkins, R.: The potential environmental response to increasing ocean alkalinity for negative
479 emissions, *Mitigation and Adaptation Strategies for Global Change*, 24, 1191-1211, 10.1007/s11027-018-9830-z, 2019.

480 Hartmann, J., Suitner, N., Lim, C., Schneider, J., Marín-Samper, L., Arístegui, J., Renforth, P., Taucher, J., and Riebesell, U.:
481 Stability of alkalinity in ocean alkalinity enhancement (OAE) approaches – consequences for durability of CO₂ storage,
482 *Biogeosciences*, 20, 781-802, 10.5194/bg-20-781-2023, 2023.

483 Hartmann, J., West, A. J., Renforth, P., Köhler, P., De La Rocha, C. L., Wolf-Gladrow, D. A., Dürr, H. H., and Scheffran, J.:
484 Enhanced chemical weathering as a geoengineering strategy to reduce atmospheric carbon dioxide, supply nutrients, and
485 mitigate ocean acidification, *Reviews of Geophysics*, 51, 113-149, 10.1002/rog.20004, 2013.

486 Hoegh-Guldberg, O., Jacob, D., Taylor, M., Guillén Bolaños, T., Bindi, M., Brown, S., Camilloni, I. A., Diedhiou, A., Djalante,
487 R., Ebi, K., Engelbrecht, F., Guiot, J., Hijjoka, Y., Mehrotra, S., Hope, C. W., Payne, A. J., Pörtner, H.-O., Seneviratne, S. I.,
488 Thomas, A., Warren, R., and Zhou, G.: The human imperative of stabilizing global climate change at 1.5 °C, *Science*, 365,
489 eaaw6974, 10.1126/science.aaw6974, 2019.

490 IPCC: Summary for Policymakers. In: *Climate Change 2021: The Physical Science Basis. Contribution of Working Group I*
491 *to the Sixth Assessment Report of the Intergovernmental Panel on Climate Change* [Masson-Delmotte, V., P. Zhai, A. Pirani,
492 S.L. Connors, C. Péan, S. Berger, N. Caud, Y. Chen, L. Goldfarb, M.I. Gomis, M. Huang, K. Leitzell, E. Lonnoy, J.B.R.
493 Matthews, T.K. Maycock, T. Waterfield, O. Yelekçi, R. Yu, and B. Zhou (eds.)], Cambridge University Press, Cambridge,
494 United Kingdom and New York, NY, USA, pp. 3-32, 10.1017/9781009157896.001, 2021.

495 Kheshgi, H. S.: Sequestering atmospheric carbon dioxide by increasing ocean alkalinity, *Energy*, 20, 915-922, 10.1016/0360-
496 5442(95)00035-F, 1995.

497 Lewis, E. L. and Perkin, R. G.: The practical salinity scale 1978: conversion of existing data, *Deep Sea Research Part A.*
498 *Oceanographic Research Papers*, 28, 307-328, 10.1016/0198-0149(81)90002-9, 1981.

499 Lioliou, M. G., Paraskeva, C. A., Koutsoukos, P. G., and Payatakes, A. C.: Heterogeneous nucleation and growth of calcium
500 carbonate on calcite and quartz, *Journal of Colloid and Interface Science*, 308, 421-428, 10.1016/j.jcis.2006.12.045, 2007.

501 [Lueker, T. J., Dickson, A. G., and Keeling, C. D.: Ocean pCO₂ calculated from dissolved inorganic carbon, alkalinity, and](#)
502 [equations for K₁ and K₂: Validation based on laboratory measurements of CO₂ in gas and seawater at equilibrium. *Marine*
503 \[Chemistry\]\(#\), 70, 105-119, 10.1016/S0304-4203\(00\)00022-0, 2000.](#)

504 Lüthi, D., Le Floch, M., Bereiter, B., Blunier, T., Barnola, J.-M., Siegenthaler, U., Raynaud, D., Jouzel, J., Fischer, H.,
505 Kawamura, K., and Stocker, T. F.: High-resolution carbon dioxide concentration record 650,000–800,000 years before present,
506 *Nature*, 453, 379-382, 10.1038/nature06949, 2008.

507 Marion, G. M., Millero, F. J., and Feistel, R.: Precipitation of solid phase calcium carbonates and their effect on application of
508 seawater SA - T - P models, *Ocean Science*, 5, 285-291, 10.5194/os-5-285-2009, 2009.

509 Millero, F., Huang, F., Zhu, X., Liu, X., and Zhang, J.-Z.: Adsorption and desorption of phosphate on calcite and aragonite in
510 seawater, *Aquatic Geochemistry*, 7, 33-56, 10.1023/A:1011344117092, 2001.

511 Monnin, E., Indermühle, A., Dällenbach, A., Flückiger, J., Stauffer, B., Stocker, T. F., Raynaud, D., and Barnola, J. M.:
512 Atmospheric CO₂ concentrations over the last glacial termination, *Science*, 291, 112-114, 10.1126/science.291.5501.112,
513 2001.

514 Montserrat, F., Renforth, P., Hartmann, J., Leermakers, M., Knops, P., and Meysman, F. J. R.: Olivine dissolution in seawater:
515 Implications for CO₂ sequestration through enhanced weathering in coastal environments, *Environmental Science &*
516 *Technology*, 51, 3960-3972, 10.1021/acs.est.6b05942, 2017.

517 Moras, C. A., Bach, L. T., Cyronak, T., Joannes-Boyau, R., and Schulz, K. G.: Ocean alkalinity enhancement – avoiding
518 runaway CaCO₃ precipitation during quick and hydrated lime dissolution, *Biogeosciences*, 19, 3537-3557, 10.5194/bg-19-
519 3537-2022, 2022.

520 Moras, C. A., Bach, L. T., Cyronak, T., Joannes-Boyau, R., and Schulz, K. G.: Preparation and quality control of in-house
521 reference materials for marine dissolved inorganic carbon and total alkalinity measurements, *Limnology and Oceanography:*
522 *Methods*, 10.1002/lom3.10570, 2023.

523 Morse, J. W., Arvidson, R. S., and Lüttge, A.: Calcium carbonate formation and dissolution, *Chemical Reviews*, 107, 342-
524 381, 10.1021/cr050358j, 2007.

525 Pan, Y., Li, Y., Ma, Q., He, H., Wang, S., Sun, Z., Cai, W.-J., Dong, B., Di, Y., Fu, W., and Chen, C.-T. A.: The role of Mg²⁺
526 in inhibiting CaCO₃ precipitation from seawater, *Marine Chemistry*, 237, 104036, 10.1016/j.marchem.2021.104036, 2021.

527 Pytkowicz, R. M.: Rates of inorganic calcium carbonate nucleation, *The Journal of Geology*, 73, 196-199, 10.1086/627056,
528 1965.

529 Sharp, J., Pierrot, D., Humphreys, M., Epitalon, J., Orr, J., Lewis, E., and Wallace, D.: CO2SYSv3 for MATLAB, Zenodo
530 [code], 10.5281/zenodo.3950562, 2021.

531 Siegenthaler, U., Stocker, T. F., Monnin, E., Lüthi, D., Schwander, J., Stauffer, B., Raynaud, D., Barnola, J. M., Fischer, H.,
532 Masson-Delmotte, V., and Jouzel, J.: Stable carbon cycle-climate relationship during the Late Pleistocene, *Science*, 310, 1313-
533 1317, 10.1126/science.1120130, 2005.

534 [Uppström, L. R.: The boron/chlorinity ratio of deep-sea water from the Pacific Ocean, *Deep Sea Research and Oceanographic*](#)
535 [Abstracts](#), 21, 161-162, 10.1016/0011-7471(74)90074-6, 1974.

536 Zeebe, R. E. and Wolf-Gladrow, D.: CO₂ in seawater: equilibrium, kinetics, isotopes, 65, Gulf Professional Publishing, 360
537 pp.2001.

538 Zhong, S. and Mucci, A.: Calcite and aragonite precipitation from seawater solutions of various salinities: Precipitation rates
539 and overgrowth compositions, *Chemical Geology*, 78, 283-299, 10.1016/0009-2541(89)90064-8, 1989.